Published in: Int. J. Mod. Phys. B**11**, 1311 – 1335 (1997).

Off-Diagonal Long-Range Order in Generalized Hubbard Models

KRISTEL MICHIELSEN AND HANS DE RAEDT

Institute for Theoretical Physics and Materials Science Centre
University of Groningen, Nijenborgh 4
NL-9747 AG Groningen, The Netherlands
E-mail: deraedt@phys.rug.nl

ABSTRACT

We present stochastic diagonalization results for the ground-state energy and the largest eigenvalue of the two-fermion density matrix of the BCS reduced Hamiltonian, the Hubbard model, and the Hubbard model with correlated hopping. The system-size dependence of this eigenvalue is used to study the existence of Off-Diagonal Long-Range Order in these models. We show that the model with correlated hopping and repulsive on-site interaction can exhibit Off-Diagonal Long-Range Order. Analytical results for some special limiting cases indicate that Off-Diagonal Long-Range Order not always implies superconductivity.

1. Introduction

In boson systems Bose-Einstein condensation is characterized by the existence of Off-Diagonal Long-Range Order (ODLRO) in the reduced one-particle density matrix.[1,2] Yang has shown that the concept of ODLRO can also be used to characterize the superconducting state of fermion systems.[3] Recently it has been shown that, under certain simplifying assumptions, ODLRO implies the existence of the Meissner effect and magnetic flux quantization.[4–6]

As pointed out by Yang, ODLRO in the reduced n-particle density matrix implies ODLRO in the reduced m-particle density matrices for all $m > n$.[3] For a fermion system the reduced density matrix of lowest order which may exhibit ODLRO is the two-body density matrix.[3] Therefore, in this paper we will confine ourselves to the study of the largest eigenvalue of the two-body density matrix. For conciseness we will use the term ODLRO, always refering to ODLRO in the two-body density matrix.

The aim of this paper is to study ODLRO in three fermion lattice models: the BCS reduced Hamiltonian, the Hubbard model and the Hubbard model with correlated hopping. Following Yang we will compute all entries of the two-particle density matrix[3]

$$\rho_{r,s} \equiv \rho(i,j,\sigma;k,l,\sigma') = \langle c^+_{i,\sigma} c^+_{j,-\sigma} c_{l,-\sigma'} c_{k,\sigma'} \rangle \quad , \tag{1}$$

where $r = (i,j,\sigma)$ and $s = (k,l,\sigma')$ and $c^+_{i,\sigma}$ and $c_{i,\sigma}$ are the creation and annihilation operators, respectively, for a fermion with spin $\sigma = \uparrow, \downarrow$ at the generalized site index i. For simplicity we will restrict ourselves to singlet pairing, as is evident from the spin labels in (1). There is ODLRO in a fermion system if the largest eigenvalue λ_0 of the $2L^2 \times 2L^2$ matrix $\rho_{r,s}$ grows linearly with the size of the system (assuming the density of particles is kept constant).[3] Accordingly a plot of λ_0 versus the system size will reveal whether or not the system exhibits ODLRO.

The outline of the paper is as follows. In section 2, we discuss the numerical techniques we use to compute the ground-state properties of the fermion lattice models and we address the difficulties that are encountered when one tries to calculate the reduced two-particle density matrix. On the one hand the computational effort required to compute the relevant physical quantities grows exponentially with the system size. On the other hand it is mandatory to have data for a number of systems of significantly different size in order for the plot of λ_0 versus the system size to be of any use at all. With these considerations in mind we decided to search for ODLRO in one-dimensional systems only.

Although in a one-dimensional model there can be no ODLRO at non-zero temperature in the strict sense,[7] at $T = 0$ there can be ODLRO even in a one-dimensional system. As the numerical method we employ is designed to compute the ground-state properties we may expect to find in our data clear signals for ODLRO whenever it is there. Due to the quantum fluctuations there can at most be "quasi" ODLRO in 1D systems with short-range interactions: The pairing correlation functions exhibit a slow (power-law) decrease for large distances, resulting in a sublinear dependence of λ_0 on L.

The eigenvector of the two-body density matrix, corresponding to λ_0, contains all the information about the type of pairing, including more exotic forms of pairing such as η pairing.[8–10] For instance, in the case of pure s-wave pairing, the elements of the eigenvector are non-zero and the same for all $r = (i,i,\sigma)$ and zero for all $r = (i,j,\sigma)$, $i \neq j$. In general, knowing this eigenvector, it is a simple matter to identify the kind of pairing that gives the dominant contribution to the ODLRO.

A presentation of the results for the three different models is given in section 3, 4 and 5 respectively. Each of these sections contains some analytical results for particular limiting cases as well as the numerical results.

2. Computational Techniques

The physical properties of a quantum system at zero temperature can be computed from the solution of the eigenvalue problem

$$H|\Phi\rangle = E|\Phi\rangle \quad , \tag{2}$$

where E denotes the smallest eigenvalue of the "matrix" H and $|\Phi\rangle$ is the corresponding eigenvector. The dimension of the matrix H will be denoted by M.

A critical factor for the selection of a method to compute E and $|\Phi\rangle$ is the amount of memory $\mathcal{M}$ needed to store $|\Phi\rangle$. For concreteness let us consider a lattice model of L sites, filled with $L/2$ electrons with spin up and $L/2$ electrons with spin down. Simple counting shows that

$$M = \binom{L}{L/2}^2 \quad , \tag{3a}$$

which for large L ($L \geq 16$ will do) can be approximated using Stirling's formula to give

$$M \approx \frac{2^{2L+2}}{2\pi L} \quad , \tag{3b}$$

demonstrating that M increases exponentially with $2L$. For instance, if $L = 16$, $M \approx 10^8$ and for $L = 64$, $M \approx 10^{35}$. Assuming that we need 8 bytes/floating point number the estimated amount of memory we need to store a single eigenvector is given by

$$\mathcal{M} \approx \frac{2^{2L-25}}{2\pi L} \text{ Gb} \quad . \tag{4}$$

From (4) it follows that $\mathcal{M} \approx 1$Gb if $L = 16$, $\mathcal{M} \approx 10^9$Gb if $L = 32$, and $\mathcal{M} \approx 10^{28}$Gb if $L = 64$.

Clearly any method that requires storage of the full matrix (i.e. $\mathcal{M} \times \mathcal{M}$ Gb will be of very limited use (as far as the range of system sizes that can be studied is concerned) to solve models for interacting fermions. Although our method of estimating the required amount of memory is somewhat crude (it does not incorporate reductions due to the use of symmetry) it gives a feeling for the kind of systems that is amenable by conventional, sparse matrix eigenvalue solvers (e.g. Lanczos, Davidson, etc.): $L = 16$ is within reach,[11–16] $L = 32$ is not.

2.1 Stochastic Diagonalization

If the dimension of the Hilbert space is so large that it is no longer feasible to store even a single vector, we make the basic assumption that of the whole, large set of basis vectors spanning the Hilbert space, only a relatively small portion is *important* when it comes to computing physical properties. This fundamental assumption is at the heart of all Quantum Monte Carlo methods currently in use.[17,18]

The stochastic diagonalization algorithm (SD) implements this idea in the following manner.[19,20] Instead of using the sparseness of the matrix, it is assumed that the solution itself is "sparse" in the sense that only a small fraction of the elements of the eigenvector, corresponding to the smallest eigenvalue, is *important*. We know that the ground state can be written as a linear combination of all the basis states $\{|\phi_j\rangle\,;\, j = 0, \ldots, M-1\}$

$$|\Phi\rangle = \sum_{j=0}^{M-1} a_j |\phi_j\rangle \quad . \tag{5}$$

In principle we can rearrange the terms in this sum so that the ones with the largest amplitude are in front:

$$|\Phi\rangle = \sum_{j=0}^{M-1} a_{Pj} |\phi_{Pj}\rangle \quad . \tag{6}$$

Here P denotes the permutation of the set $\{0, \ldots, M-1\}$ such that $|a_{Pj}| \geq |a_{P(j+1)}|$. Assuming that we obtain a good approximation if we restrict the sum to the first M_I terms we have

$$|\Phi\rangle \approx |\widetilde{\Phi}\rangle = \sum_{j=0}^{M_I} a_{Pj} |\phi_{Pj}\rangle \quad . \tag{7}$$

According to the Poincaré theorem[21,22] we have

$$E \leq \widetilde{E} = \frac{\langle\widetilde{\Phi}|H|\widetilde{\Phi}\rangle}{\langle\widetilde{\Phi}|\widetilde{\Phi}\rangle} \quad , \tag{8}$$

demonstrating that stochastic diagonalization belongs to the class of variational techniques. By virtue of the basic assumption we expect that $M_I \ll M$. In practice M_I will depend on the actual choice of the basis vectors (i.e. the representation used) and on the model itself.

Up to know, we have assumed that we know the permutation P that does the job described above, but in fact we don't know P nor do we know the coefficients a_{Pj}. The SD method uses a stochastic process to construct P and the coefficients

a_{Pj} simultaneously. Thereby it does not suffer from the so-called minus-sign problem that is usually encountered in Quantum Monte Carlo (QMC) work.[18,20,23] A further advantage of the SD method is that it can deal with more complicated lattice models (see below) than those amenable to QMC techniques. Albeit at much greater expense, the SD method yields exact results whenever other methods (such as Lanczos) will, because then we can store the whole vector and put $M_I = M$ from the start. A rigorous proof of the correctness of the SD algorithm, an extensive discussion on the origin of the minus-sign problem, and details on the implementation of the SD algorithm can be found elsewhere.[20]

As usual the symmetries of the model system can be used to reduce the actual size of the Hilbert space, resulting in a more efficient computational method. In all our numerical work we adopt periodic boundary conditions. Our SD codes work either with the real-space or Fourier space representation and can take advantage of the spatial and spin symmetries of the model.

Most of the data presented in this paper have been obtained from runs that use all obvious tricks to reduce the size of the Hilbert space. For many of the systems studied, the calculations were carried out using both representations, providing a highly non-trivial consistency check. Occasionally some runs have been repeated without the use of symmetries. For small systems, the results of the SD calculations have been compared against those obtained from exact diagonalization and, as expected on theoretical grounds, no differences were found.

2.2 Computation of physical properties

Assuming the ground state has been found, either in exact form by e.g. the Lanczos method or in the variational sense through the SD algorithm, a calculation of the expectation values of physical quantities may become a non-trivial computational problem if the matrix representing the observable is not diagonal in the basis that was used to represent the Hamiltonian. Indeed, if A denotes the physical observable, the expectation value of A is given by

$$\langle A \rangle = \langle \Phi | A | \Phi \rangle = \sum_{i,j=0}^{M-1} a_i a_j \langle \phi_i | A | \phi_j \rangle \quad , \tag{9}$$

showing that in general it will take $\mathcal{O}(M^2)$ operations to carry out this computation. For large M, it may take longer to calculate certain expectation values than it takes to solve for the ground state itself and in fact, for some of the examples to be discussed below, this is indeed the case.

The calculation of the ground-state energy itself does not require extra work because (the approximation to) it is known at each stage of the SD process.[20] However the evaluation of the two-particle density matrix (1) is time consuming.

The number of operations in the algorithm that we use to compute all entries of this matrix scales with LM_I^2. For most of the systems that we have studied $M_I = \mathcal{O}(10^5)$, indicating that the CPU time required to set up the two-particle density matrix can be substantial.

As an independent check on the results obtained from the two-particle density matrix we also compute the on-site (s-wave) pairing correlation function

$$P_0 \equiv \frac{1}{L} \sum_{i,j} \langle c_{i,\uparrow}^+ c_{i,\downarrow}^+ c_{j,\downarrow} c_{j,\uparrow} \rangle \quad . \tag{10}$$

As the contributions to P_0 appear on the diagonal of the two-particle density matrix (1) we must have

$$P_0 \leq \lambda_0 \quad , \tag{11}$$

an inequality that is never violated by our numerical data. From (11) it is clear that there is ODLRO if $P_0 \propto L$ for large L, i.e. ODLRO of the on-site type.

Another simple check on the numerical results is provided by the rigorous upperbound to λ_0, given by Yang[3], which for the case at hand can be written as

$$\lambda_0 \leq L \frac{n(2-n)}{2} + n \quad ; \quad nL \quad \text{even} \quad . \tag{12}$$

where

$$n = L^{-1} \sum_{i,\sigma} \langle n_{i,\sigma} \rangle \quad , \tag{13}$$

denotes the density of particles. All our numerical results are also in concert with (12).

Other criteria which may be used to decide whether or not a given model exhibits superconductivity is the occurrence of flux quantization[3,24] or a non-zero value of the superfluid density ρ_s.[25]

To explore flux quantization we thread a magnetic flux ϕ through the center of the ring. As a consequence the hopping term in the model Hamiltonian acquires a constant phase $\exp(\pm 2\pi i \phi / L\phi_0)$ where $\phi_0 = hc/e$ is the flux quantum.[26] Byers and Yang argue that, in the thermodynamic limit, the functional form of the free energy $F(\phi) = -\beta^{-1} \ln \mathbf{Tr}\ e^{-\beta H}$ as a function of ϕ allows one to distinguish between a normal metal and a superconductor.[3,24] In the case of a superconductor $F(\phi)$ is an even periodic function of ϕ with period ϕ_0/k where k stands for the sum of charges of the particles in the basic group.[3] The resulting flux dependence requires that a superconductor exhibits ODLRO.[3] On the other hand, the curve $F(\phi)$ is flat in the case of a normal metal.

In Fig.1 we plot the energy difference $\Delta E(\phi) \equiv E(\phi) - E(\phi = 0)$ (at zero-

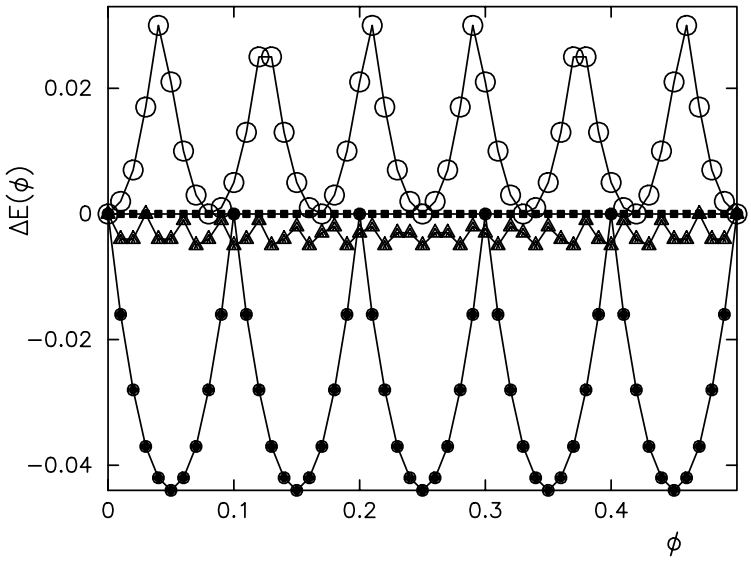

Fig.1. $\Delta E(\phi)$ for free fermions at zero temperature. Bullets: 12-site ring; circles: 14-site ring; triangles: 36-site ring; squares: 128-site ring. The lines are guides to the eye.

temperature $F(\phi) = E(\phi)$, $E(\phi)$ being the ground-state energy for a given ϕ) for free fermions on a ring of 12 (bullets), 14 (circles), 36 (triangles) and 128 (squares) sites. For small systems $\Delta E(\phi)$ clearly exhibits periodic behavior as a function of ϕ. This implies the presence of persistent currents ($J \propto \partial E/\partial\phi$), a well-known phenomenon in mesoscopic normal-metal rings.[27−30] Also clear from Fig.1 is that the signal for flux quantization strongly depends on system-size: Only for a ring of 128 sites $\Delta E(\phi)$ is flat (up to four digits at least). Because of these finite-size effects and the fact that it is difficult to solve numerically interacting fermion systems on large lattices, we decided not to use flux quantization as a criterion to decide whether or not the system exhibits ODLRO.

The superfluid density ρ_s can be calculated from the dependence of the free energy on ϕ using $\rho_s \propto L^{-1}(\partial^2 F(\phi/L)/\partial(\phi/L)^2)_{\phi/L=0}$.[31−34] A feeling for the system-size dependence of ρ_s can be obtained by considering a free electron system. Evidently in that case one expects to find $\rho_s = 0$, independent of the dimension and the temperature. For a one-dimensional free electron system[35]

$$\left.\frac{\partial^2 F}{\partial(\phi/L)^2}\right|_{\phi/L=0} = 2t\sum_k n_k \cos k - 2\beta t \sum_k n_k(1-n_k)\sin^2 k \quad , \tag{14}$$

with

$$n_k = \frac{1}{e^{\beta(-2t\cos k-\mu)}+1} \quad , \tag{15}$$

where t denotes the hopping integral, β the inverse temperature, and μ the chemical potential.

L	$\beta = 10$	$\beta = 100$	$\beta = 1000$
16	-0.626	-11.872	-124.37
18	0.386	0.640	0.639
32	-0.087	-5.615	-61.865
34	0.066	0.638	0.638
36	-0.052	-4.921	-54.921
64	-0.001	-2.489	-30.614
66	0.001	0.635	0.637
72	0.000	-2.141	-27.142
1024	0.000	0.000	-1.312
1026	0.000	0.000	0.603
10000	0.000	0.000	0.000

Table 1. Superfluid density ρ_s for the half-filled one-dimensional free electron system as a function of system size L and inverse temperature β.

Numerical results for the r.h.s. of (14) for various system sizes and inverse temperatures for $t = 1$ and $n = 1$ are given in Table 1. For all temperatures $\rho_s \leq 0$ for $L = 4m$ and $\rho_s \geq 0$ for $L = 4m+2$ where m is an integer number. This change of sign of ρ_s with L is similar to the behavior found in the Drude weight.[36,37] At very low temperatures very large system sizes are needed to obtain $\rho_s = 0$, as required for the free electron system.[38] The system size required to yield a vanishing ρ_s grows with the inverse temperature, a feature which makes it difficult to use as a criterion for superconductivity a non-zero value for ρ_s.

3. BCS reduced Hamiltonian

From pedagogical viewpoint it is important to have at least one example for which it is known that the system supports ODLRO. Such an example is provided by the Hamiltonian

$$H^{BCS} = -t \sum_{\langle i,j \rangle} \sum_{\sigma=\uparrow,\downarrow} \left(c^+_{i,\sigma} c_{j,\sigma} + c^+_{j,\sigma} c_{i,\sigma} \right) - \frac{|U|}{L} \sum_{i,j} c^+_{i,\uparrow} c^+_{i,\downarrow} c_{j,\downarrow} c_{j,\uparrow} \quad . \tag{16}$$

where $c^+_{i,\sigma}$ and $c_{i,\sigma}$ are the creation and annihilation operators, respectively, for a fermion with spin $\sigma =\uparrow,\downarrow$ at the site (or orbital) i and the sum over $\langle i,j \rangle$ is

over distinct pairs of nearest neighbor lattice sites on a chain of length L. t is the hopping parameter and U is the on-site pairing interaction. A variational, BCS-like treatment of (16) yields the exact solution,[39] hence the name "BCS reduced Hamiltonian". As ODLRO is a characteristic feature of the BCS wave function,[3] any numerical method that solves (16) should be able to reproduce this feature.

In the Fourier representation (16) reads

$$H^{BCS} = \sum_k \sum_{\sigma=\uparrow,\downarrow} \epsilon_k \, c^+_{k,\sigma} c_{k,\sigma} - \frac{|U|}{L} \sum_{k,p} c^+_{k,\uparrow} c^+_{-k,\downarrow} c_{-p,\downarrow} c_{p,\uparrow} \quad , \tag{17}$$

where $\epsilon_k = -2t \cos k$.

3.1 BCS approximation

The BCS treatment consists of invoking the variational principle to minimize the upperbound to the grand potential $\Omega = -\beta^{-1} \ln \mathbf{Tr} \, \exp(-\beta(H - \mu N))$, where $N = \sum_{i,\sigma} c^+_{i,\sigma} c_{i,\sigma} = \sum_{i,\sigma} n_{i,\sigma}$ the number of particles. The inequality for Ω reads

$$\Omega \leq \Omega^{trial} + \langle H - \mu N - H^{trial} \rangle^{trial} \quad , \tag{18}$$

where $\langle X \rangle^{trial}$ is the thermal expectation value of the observable X with respect to the ensemble defined by H^{trial} and $\Omega^{trial} = -\beta^{-1} \ln \mathbf{Tr} \, \exp(-\beta H^{trial})$ for a trial Hamiltonian of the form

$$H^{trial} = \sum_k \sum_{\sigma=\uparrow,\downarrow} E_k \, c^+_{k,\sigma} c_{k,\sigma} + \Delta \sum_k \left(c^+_{k,\uparrow} c^+_{-k,\downarrow} + c_{-k,\downarrow} c_{k,\uparrow} \right) \quad . \tag{19}$$

For model (16) and at zero temperature ($\beta = \infty$), the resulting equations for E_k and Δ read

$$E_k = \epsilon_k - \widetilde{\mu} + \frac{|U|}{2L} \frac{E_k}{\sqrt{E_k^2 + \Delta^2}} \quad , \tag{20a}$$

and

$$1 = \frac{|U|}{2L} \sum_k \frac{1}{\sqrt{E_k^2 + \Delta^2}} \quad , \tag{20b}$$

where the chemical potential μ and some irrelevant constants have been absorbed in $\widetilde{\mu}$. The latter is determined by the requirement that the averaged density of particles is equal to the specified particle density, i.e.

$$n = 1 - \frac{1}{L} \sum_k \frac{E_k}{\sqrt{E_k^2 + \Delta^2}} \quad . \tag{21}$$

In the thermodynamic limit $L \to \infty$, the last term in (20a) vanishes and (20b) reduces to the standard BCS gap equation,[40] as expected on the basis of the rigorous treatment of model (16).[39]

The on-site pairing correlation function P_0 is given by

$$P_0^{BCS} = \frac{1}{4L} \sum_k \left(1 - \frac{E_k}{\sqrt{E_k^2 + \Delta^2}} \right)^2 + \frac{\Delta^2}{4L} \left(\sum_k \frac{1}{\sqrt{E_k^2 + \Delta^2}} \right)^2 \quad . \tag{22}$$

With the use of equations (20b) and (21), we find

$$P_0^{BCS} = \frac{n}{2} - \frac{\Delta^2}{4L} \sum_k \frac{1}{E_k^2 + \Delta^2} + \frac{L\Delta^2}{U^2} \quad , \tag{23}$$

explicitly showing that the ground state of H^{BCS} exhibits ODLRO of the on-site (s-wave) type.

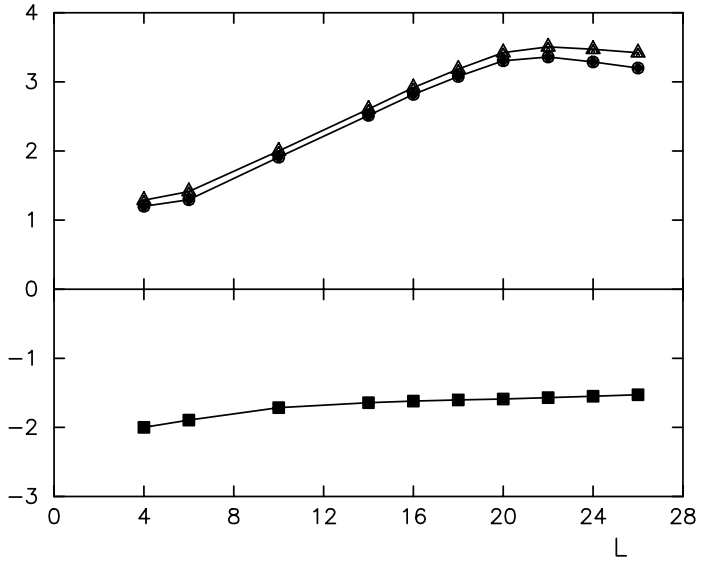

Fig.2. Ground-state energy per site E/L, on-site pairing correlation function P_0 and largest eigenvalue λ_0 of the reduced two-particle density matrix as a function of system size L for the BCS reduced Hamiltonian for $t = 1$, $U = -4$ and $n = 1$. Squares: E/L; bullets: P_0; triangles: λ_0. The lines are guides to the eye.

3.2 Numerical results

Numerical results for the ground-state energy per site E/L, the on-site pairing correlation function P_0 and the largest eigenvalue λ_0 of the two-particle density matrix as a function of system size for half-filled rings are shown in Fig.2. For small system sizes E/L increases with L. For $L \geq 14$ the L-dependence of the ground-state energy is no longer visible on the scale used in Fig.2. For $6 \leq L < 22$ the largest eigenvalue λ_0 of the two-particle density matrix grows linearly with L, as expected since the system described by Hamiltonian (16) exhibits ODLRO.[39] For larger system sizes λ_0 decreases, indicating that the number of important states M_I that can be taken into account is too small for these system sizes. The number of important states M_I collected by the SD algorithm, working in the Fourier space representation, varies from $M_I \approx 6$ for $L = 4$ to $M_I \approx 100000$ for $L \geq 22$. The dimension of the Hilbert space varies from $M = 36$ for $L = 4$ to $M \approx 10^{14}$ for $L = 26$. The behavior of P_0 and λ_0 as a function of system size is identical, as expected in this case. Hence, the ODLRO exhibited by the system is mainly of the on-site (s-wave) pairing type.

Studying the ground-state energy and physical properties as a function of the number of important states shows that convergence of the ground-state energy does not guarantee convergence of other physical poperties. For example, in Table 2 we show the ground-state energy per site and λ_0 as a function of the number of important states M_I collected by the SD algorithm for an 18-site ring. In this case the dimension of the Hilbert space $M \approx 2.3\,10^9$. We find a 2-digit accuracy in the energy for $M_I \geq 15000$, while for λ_0 we need at least 30000 states to get a 2-digit accuracy.

M_I	E/L	λ_0
8119	-1.587	2.731
15137	-1.597	3.001
19618	-1.600	3.081
23056	-1.601	3.127
26027	-1.602	3.150
28504	-1.602	3.167
45657	-1.603	3.176
48519	-1.603	3.184

Table 2. Ground-state energy per site E/L and largest eigenvalue λ_0 of the reduced two-particle density matrix as a function of the number of important states M_I for the BCS reduced Hamiltonian for $L = 18$, $t = 1$, $U = -4$ and $n = 1$.

4. The Hubbard model

The Hubbard model is described by the Hamiltonian[41]

$$H^{Hub} = -t \sum_{\langle i,j \rangle} \sum_{\sigma=\uparrow,\downarrow} \left(c^+_{i,\sigma} c_{j,\sigma} + c^+_{j,\sigma} c_{i,\sigma} \right) + U \sum_i c^+_{i,\uparrow} c^+_{i,\downarrow} c_{i,\downarrow} c_{i,\uparrow} \quad . \tag{24}$$

where U is the on-site Coulomb interaction. In the Fourier representation (24) reads

$$H^{Hub} = \sum_k \sum_{\sigma=\uparrow,\downarrow} \epsilon_k \, c^+_{k,\sigma} c_{k,\sigma} + \frac{U}{L} \sum_{k,p,q} c^+_{k+q,\uparrow} c^+_{p-q,\downarrow} c_{p,\downarrow} c_{k,\uparrow} \quad . \tag{25}$$

The Hubbard model is the generic model for the description of electron correlations in narrow energy-band systems and, because of its apparent simplicity, is often the model of choice for numerical work on correlated electron systems. Unfortunately, this simplicity is somewhat misleading in this respect too: Simulating a Hubbard model is not a simple matter.[18]

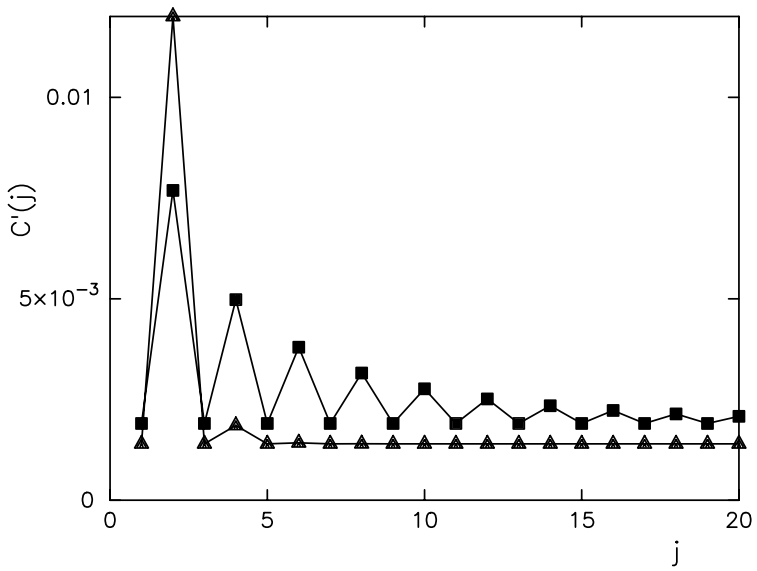

Fig.3. Pairing correlation function $C'(j)$ as a function of distance j between the electrons in a pair for the Hubbard model in the BCS approximation for $t = 1$ and $n = 1.5$. Squares: $U = -0.2$; triangles: $U = -4$. For clarity, the large on-site contribution at $j = 0$ is left out. The lines are guides to the eye.

4.1 BCS treatment

The BCS treatment of H^{Hub} is almost identical to that of H^{BCS}. We only give it here for the sake of completeness. At $T = 0$ the equations for the quasi-particle energy and the gap read

$$E_k = \epsilon_k - \widetilde{\mu} \quad , \tag{26a}$$

and

$$1 = -\frac{U}{2L}\sum_k \frac{1}{\sqrt{E_k^2 + \Delta^2}} \quad , \tag{26b}$$

showing that in the thermodynamic limit and within the BCS treatment, the ground-state properties of H^{BCS} and H^{Hub} are identical, provided $U < 0$ (i.e. in the case of the attractive Hubbard model). In particular, at zero temperature

$$\frac{\langle H^{Hub}\rangle^{trial}}{L} = \frac{\langle H^{BCS}\rangle^{trial}}{L} + \frac{Un^2}{4} \quad . \tag{27}$$

Since H^{BCS} exhibits ODLRO of the on-site type also H^{Hub} shows ODLRO of the on-site type for $U < 0$, $T = 0$ and $L \to \infty$.

An indication of the finite-size effects can be given by studying the size of an electron pair. Therefore we show in Fig.3 the pairing correlation function

$$C'(j) = \frac{1}{L^2}\sum_{i,l}\langle c^+_{i,\uparrow}c^+_{i+j,\downarrow}c_{l+j,\downarrow}c_{l,\uparrow}\rangle \quad , \tag{28}$$

for attractive ($U = -0.2$ and $U = -4$) three-quarter filled Hubbard rings of 256 sites in the BCS approximation. For $U = -0.2$ an electron pair extends over several lattice sites while for $U = -4$ the size of an electron pair is much smaller. This indicates that, because of the large system sizes needed, numerically it may be very difficult to detect ODLRO in the Hubbard model for small negative U.

To compare the results of the BCS treatment with the numerical results obtained by SD, we solve (21) and (26b) numerically for finite L. In the BCS treatment the number of particles is allowed to fluctuate whereas in the SD calculations the number of particles is fixed. Therefore some (finite-size) differences between the SD and BCS-treatment data may be expected, due to the different ensembles used. Some representative results for $U = -4$ are shown in Table 3. From Table 3 it is clear that the SD algorithm yields a better upperbound to the ground-state energy of the Hubbard model than the BCS treatment does.

It is of interest to consider the limit $t \to 0$ and a half-filled system $n = 1$. Solving (21) and (26b) at zero temperature for $t \to 0$, $U < 0$, and $n = 1$ yields

L	$\langle H^{Hub}\rangle^{trial}/L$	$\langle H^{Hub}\rangle/L$
6	-2.472	-2.611
10	-2.469	-2.583
14	-2.469	-2.557
18	-2.469	-2.534
22	-2.469	-2.499

Table 3. Comparison between the ground-state energy of the Hubbard model for $U=-4$, $t=1$ and $n=1$ as obtained from the BCS treatment and SD.

$\widetilde{\mu}=0$, $2\Delta=|U|$, and

$$E=\frac{\langle H^{Hub}\rangle^{trial}}{L}=-\frac{|U|}{2} \quad ; \quad P_0=\frac{L+1}{4} \quad , \tag{29}$$

showing that in this limit, the BCS treatment reproduces the exact ground-state energy of the attractive Hubbard model in the atomic limit and, as expected from the BCS treatment, also ODLRO.

4.2 Atomic limit

We now consider the extreme case where we put $t=0$ from the start and take $U<0$. Then, for any filling with $\sum_i\langle n_{i,\uparrow}\rangle=\sum_i\langle n_{i,\downarrow}\rangle$, the ground state is $\binom{L}{N/2}$-fold degenerate. Any linear combination of states, each one describing $N/2$ pairs of spin-up and spin-down particles, qualifies as a ground state and has a ground-state energy $-|U|n/2$. Can some of these linear combinations exhibit ODLRO?

This question can be answered by adding to the Hamiltonian a term that does not conserve the number of particles. In analogy with the BCS treatment we write

$$H^{atom}=-|U|\sum_i c^+_{i,\uparrow}c^+_{i,\downarrow}c_{i,\downarrow}c_{i,\uparrow}+\Delta\sum_i\left(c^+_{i,\uparrow}c^+_{i,\downarrow}+c_{i,\downarrow}c_{i,\uparrow}\right) \quad . \tag{30}$$

For simplicity we now restrict ourselves to the half-filled band case. Then the energy and the on-site pairing correlation function are given by

$$E^{atom}=-\frac{|U|}{2}+\frac{|U|e^{-\beta|U|/2}-2\Delta\sinh\beta\Delta}{2e^{-\beta|U|/2}+\cosh\beta\Delta} \quad , \tag{31a}$$

and

$$P_0^{atom} = \frac{(L-1)}{4}\left(\frac{\sinh\beta\Delta}{e^{-\beta|U|/2}+\cosh\beta\Delta}\right)^2 + \frac{1}{2}\frac{\cosh\beta\Delta}{\left(e^{-\beta|U|/2}+\cosh\beta\Delta\right)} \quad , \quad (31b)$$

respectively. From (31) we find that

$$\lim_{\Delta\to 0}\lim_{\beta\to\infty} E^{atom} = -\frac{|U|}{2} = \lim_{\beta\to\infty}\lim_{\Delta\to 0} E^{atom} = -\frac{|U|}{2} \quad , \qquad (32a)$$

whereas

$$\lim_{\Delta\to 0}\lim_{\beta\to\infty} P_0^{atom} = \frac{L+1}{4} \neq \lim_{\beta\to\infty}\lim_{\Delta\to 0} P_0^{atom} = \frac{1}{2} \quad , \qquad (32b)$$

showing that, depending on the order in which the two limits are taken, in the atomic limit the attractive Hubbard model will exhibit ODLRO, in concert with the result of the BCS treatment (see (29)). In the absence of hopping, there can be no flow of particles and hence no superconductivity. We find that in this highly degenerate case, ODLRO does not imply superconductivity.

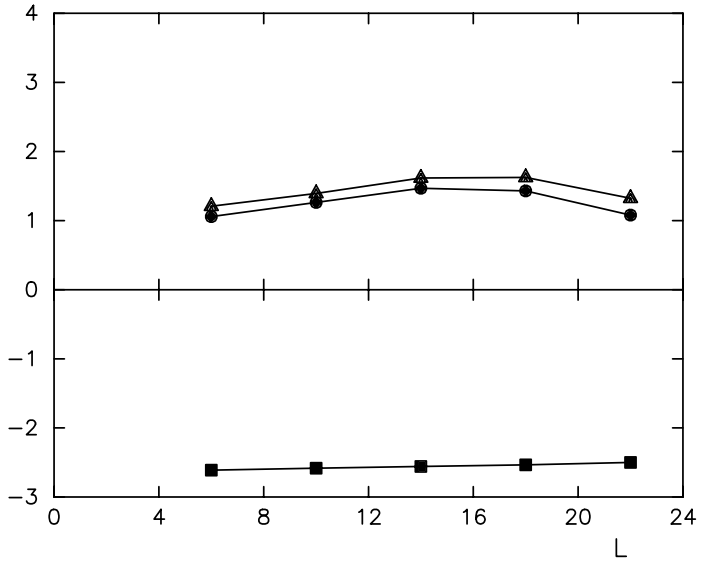

Fig.4. Ground-state energy per site E/L, on-site pairing correlation function P_0 and largest eigenvalue λ_0 of the reduced two-particle density matrix as a function of system size L for the Hubbard model for $t = 1$, $U = -4$ and $n = 1$. Squares: E/L; bullets: P_0; triangles: λ_0. The lines are guides to the eye.

4.3 Numerical results

Numerical results for the ground-state energy per site E/L, the on-site pairing correlation function P_0 and the largest eigenvalue λ_0 of the two-particle density matrix as a function of system size for the half-filled attractive Hubbard model are shown in Fig.4. The ground-state energy does not strongly depend on system size for the system sizes studied here. For $6 \leq L < 18$ the largest eigenvalue λ_0 of the two-particle density matrix grows with L. This points to ODLRO. For larger system sizes λ_0 decreases, indicating that, in analogy with the results on the BCS reduced Hamiltonian, the number of important states M_I that can be taken into account may be too small for these system sizes. The number of important states M_I collected by the SD algorithm, working in the Fourier space representation, varies from $M_I \approx 68$ for $L = 6$ to $M_I \approx 197000$ for $L \geq 18$. The dimension of the Hilbert space varies from $M = 400$ for $L = 6$ to $M \approx 2.8\,10^{11}$. for $L = 22$. The behavior of P_0 as a function of system size is identical to the behavior of λ_0 as a function of system size but $P_0 \neq \lambda_0$. Hence, the ODLRO exhibited by the system is mainly of the on-site (s-wave) pairing type.

In Table 4 we show E/L and λ_0 as a function of the number of important states M_I for a ring with 18 sites. Comparing Table 2 and Table 4 shows that for the attractive Hubbard model we need much more important states to get convergence in the energy and λ_0 than for the BCS reduced Hamiltonian. Hence, for $L \geq 18$ the number of states is too small to decide whether or not there is ODLRO.

M_I	E/L	λ_0
37417	-2.520	1.691
56731	-2.523	1.686
91603	-2.527	1.663
196186	-2.534	1.624

Table 4. Ground-state energy per site E/L and largest eigenvalue λ_0 of the reduced two-particle density matrix as a function of the number of important states M_I for the Hubbard Hamiltonian for $L = 18$, $t = 1$, $U = -4$ and $n = 1$.

An indication for the presence of ODLRO can also be found by looking at the distance-dependence of pairing correlation functions for systems of different size. The on-site pairing correlation function

$$C(j) = \frac{1}{L} \sum_i \langle c^+_{i,\uparrow} c^+_{i,\downarrow} c_{i+j,\downarrow} c_{i+j,\uparrow} \rangle \quad , \tag{33}$$

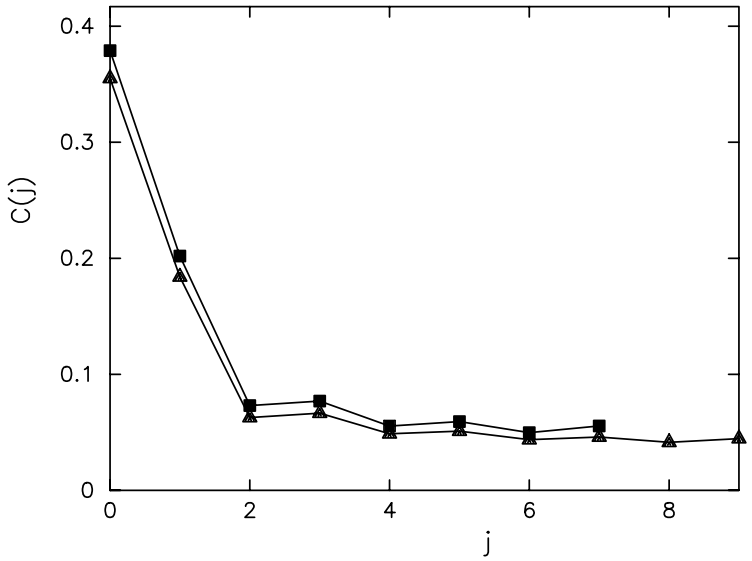

Fig.5. On-site pairing correlation function $C(j)$ as a function of distance j for the Hubbard model for $t = 1$, $U = -4$ and $n = 1$. Squares: 14-site ring; triangles: 18-site ring. The lines are guides to the eye.

for attractive ($U = -4$) Hubbard rings of 14 and 18 sites is shown in Fig.5. In Quantum Monte Carlo work the saturation of $C(j)$ with increasing distance is often taken as evidence of the presence of ODLRO in the system.

The SD results shown above all indicate ODLRO. That this is not an artifact of the method can be ruled out by repeating the calculation for the repulsive Hubbard model. Numerical results for the ground-state energy per site E/L, the on-site pairing correlation function P_0 and the largest eigenvalue λ_0 of the two-particle density matrix as a function of system size for the half-filled repulsive Hubbard model are shown in Fig. 6. The number of important states M_I collected by the SD algorithm, working in the Fourier space representation, is $M_I \approx 198000$ for $L = 14$ (for which $M \approx 1.2\,10^6$). For $L \leq 14$ the ground-state energy increases slightly with the size of the system. The largest eigenvalue λ_0 of the two-particle density matrix and the on-site pairing correlation function decrease with the system size, for the system sizes studied here. Hence, at half-filling the repulsive Hubbard model ($U = 4$) does not show ODLRO, as is well known.

To give an indication for the finite-size effects we show in Fig.7 λ_0 as a function of system size for the three-quarter filled Hubbard model for $U = -4$, $U = -0.2$, $U = 0.2$ and $U = 4$. For $U > 0$, λ_0 does not increase with the system size. Hence, also the 1D three-quarter filled Hubbard model does not show ODLRO, as expected. For large negative U ($U = -4$ for example) λ_0 grows with L. This points to ODLRO. For $U = -0.2$ there is no noticeable increase of λ_0 with L. As seen in section 4.1, the BCS approximation to the Hubbard model shows that for $U = -0.2$

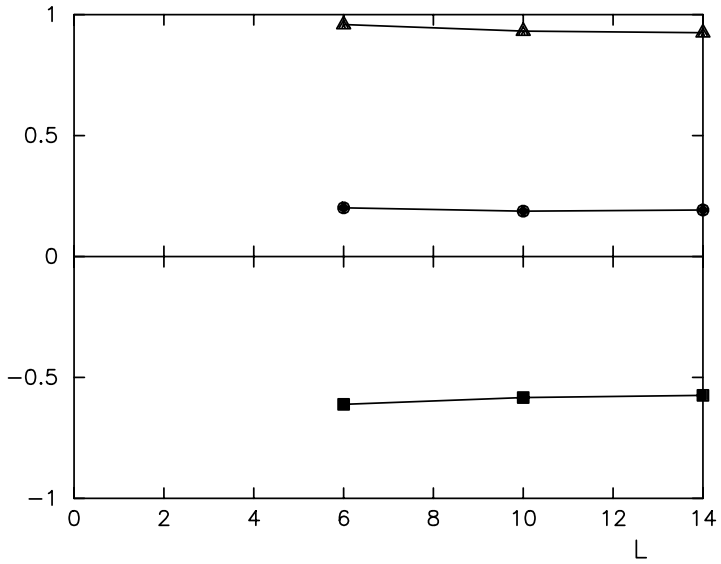

Fig.6. Ground-state energy per site E/L, on-site pairing correlation function P_0 and largest eigenvalue λ_0 of the reduced two-particle density matrix as a function of system size L for the Hubbard model for $t = 1$, $U = 4$ and $n = 1$. Squares: E/L; bullets: P_0; triangles: λ_0. The lines are guides to the eye.

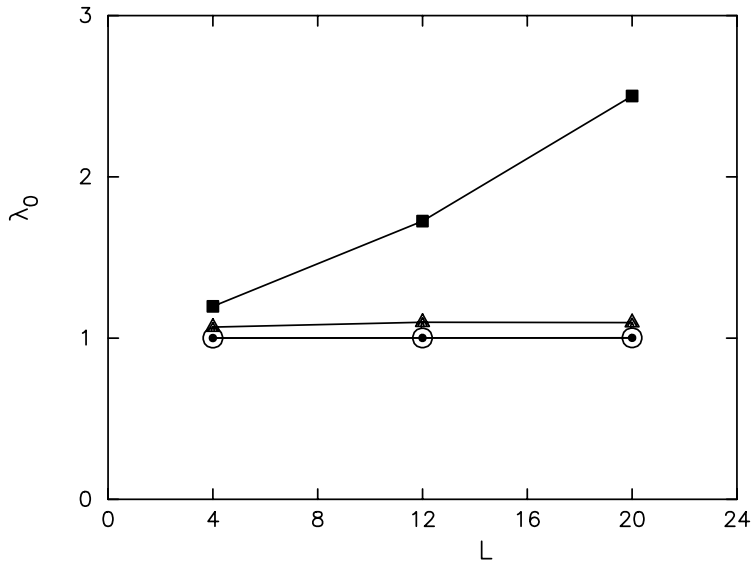

Fig.7. Largest eigenvalue λ_0 of the reduced two-particle density matrix as a function of system size L for the Hubbard model for $t = 1$ and $n = 1.5$. Squares: $U = -4$; bullets: $U = -0.2$; circles: $U = 0.2$; triangles: $U = 4$. The lines are guides to the eye.

the size of an electron pair is much larger than the length of the rings we can study

with the SD method, while for $U = -4$ the size of an electron pair is approximately one lattice site. Hence, due to these finite-size effects for small negative U, our numerical results cannot show the characteristic signal of ODLRO.

5. Hubbard model with correlated hopping

The tight binding Hamiltonian (for a single band) as derived by Hubbard includes different interaction terms.[41] Keeping only the nearest-neighbor interactions there are several contributions: $U = (ii|1/r|ii)$, $V = (ij|1/r|ij)$, $\Delta t = (ii|1/r|ij)$ and $X = (ii|1/r|jj)$. The Hubbard integrals U (on-site) and V (inter-site) are the energies of the interactions between electrons at the same site and neighboring sites, respectively. The correlated hopping interaction Δt describes the interaction between electrons localized on a given site and on the bond directed to a neighboring site and is therefore also called the bond-charge site-charge interaction. The integral X is the energy of the interaction between electrons on the same bond. We will consider the case $V = X = 0$. Then the Hamiltonian reads[41]

$$H = H^{Hub} + \Delta t \sum_{<i,j>} \sum_{\sigma} \left(n_{i,-\sigma} + n_{j,-\sigma}\right) \left(c^{+}_{i,\sigma} c_{j,\sigma} + c^{+}_{j,\sigma} c_{i,\sigma}\right) \quad . \tag{34}$$

Fourier transformation of each of the contributions to (34) yields

$$\begin{aligned} H = & \sum_{k} \sum_{\sigma=\uparrow,\downarrow} \epsilon_k \, c^{+}_{k,\sigma} c_{k,\sigma} \\ & + \frac{1}{L} \sum_{k,p,q} \left[U - t^{-1} \Delta t (\epsilon_k \, + \epsilon_{k+q})\right] c^{+}_{k+q,\uparrow} c^{+}_{p-q,\downarrow} c_{p,\downarrow} c_{k,\uparrow} \quad . \end{aligned} \tag{35}$$

This model was first studied by Caron and Pratt using a self-consistent cluster treatment.[42] Recently, the exact ground state of the model at half-filling (including V) for $\Delta t = t$ has been found for any dimension and a wide range of parameters.[43,44] In one dimension the model can also be solved exactly away from half-filling for the special case $\Delta t = t$.[44–46] In more than one dimension the qualitative form of the ground-state phase diagram for $\Delta t = t$ is basically the same as that of the ground-state phase diagram in one dimension although the exact location of all phase boundaries cannot be determined.[46] Exact diagonalization for chains up to 12 sites[47] and weak-coupling continuum-limit calculations,[48] provide additional information on (part of) the ground-state phase diagram.

It has been suggested that the correlated hopping interaction is essential for the occurrence of superconductivity.[49,50] The Hubbard model with correlated hopping is an effective one-band model for the CuO_2-planes of cuprate superconductors[51–53] and has been studied by a cluster effective-medium approach,[54] generalized mean-field techniques,[55–57] and BCS calculations.[58–60] It has also been shown that

model (34) has η-pairs in the ground state and that the η-pairing states have ODLRO.[45,46,61] Recently it has been demonstrated that the ODLRO of the η-paired states is not a sufficient condition for the existence of superconductivity.[62]

Adding spin-flip hopping processes, it is possible to obtain the static and dynamic properties of the model and hence a complete picture of the full $(n, \Delta t/t, U/t)$ phase diagram.[63–70] For $\Delta t = t$ the qualitative form of the ground-state phase diagram is similar to the ground-state phase diagram of model (34) and the dimensionality of the lattice does not play an important role. From the phase diagram it follows that for $\Delta t = t$ as well as model (34) as model (34) with spin-flip hopping processes exhibit a continuous Mott metal-insulator transition at $n = 1$, $U = 4d|t|$ where d is the lattice dimensionality. For $0 < \Delta t < t$ model (34) with spin-flip hopping processes has a discontinuous metal-insulator transition at half-filling.

5.1 BCS treatment

As a trial Hamiltonian we adopt

$$H^{trial} = \sum_{k} \sum_{\sigma} E_k \, c^{+}_{k,\sigma} c_{k,\sigma} + \sum_{k} \left(\Delta_k \, c^{+}_{k,\uparrow} c^{+}_{-k,\downarrow} + \Delta_k \, c_{-k,\downarrow} c_{k,\uparrow} \right) \quad , \tag{36}$$

where, in contrast to the cases discussed above, the gap Δ_k depends on the wave vector k. Without loss of generality we have assumed that Δ_k is real and for the sake of brevity, we only give results for the one-dimensional case.

Minimizing the upperbound to the grand potential gives

$$E_k = -\, 2(t - n\Delta t) \cos k - \widetilde{\mu} - \frac{2\Delta t}{L} \sum_{p} E_p f_p \cos p \quad , \tag{37a}$$

and

$$\Delta_k = -\, \frac{U + 4\Delta t \cos k}{2L} \sum_{p} \Delta_p f_p - \frac{2\Delta t}{L} \sum_{p} \Delta_p f_p \cos p \quad , \tag{37b}$$

where, for zero temperature, $f_k = (E_k^2 + \Delta_k^2)^{-1/2}$. From (37b) it follows the k-dependence of the gap can be written as $\Delta_k = a + b \cos k$ and we obtain

$$b = -\, \frac{2aF_0 \Delta t}{1 + 2F_1 \Delta t} \quad , \tag{38a}$$

and

$$1 = -\, \frac{UF_0}{2} - 4F_1 \Delta t - (2\Delta t)^2 (F_1^2 - F_0 F_2) \quad , \tag{38b}$$

where $F_n \equiv L^{-1} \sum_k \cos^n k f_k$.

Within the BCS treatment, the ground-state energy is given by

$$E = 2\,(t - n\Delta t) \sum_k E_k f_k \cos k + \frac{U}{4} n^2 L + \frac{U}{4L} \left(\sum_k \Delta_k f_k \right)^2 + \frac{2\Delta t}{L} \left(\sum_k \Delta_k f_k \cos k \right) \left(\sum_k \Delta_k f_k \right) \quad , \tag{39}$$

and the on-site pairing correlation function reads

$$P_0 = \frac{1}{4L} \sum_k \left(1 - E_k f_k\right)^2 + \frac{1}{4L} \left(\sum_k \Delta_k f_k \right)^2 \quad . \tag{40}$$

There are now two ways to proceed. Non-trivial numerical work is necessary to solve the set of non-linear equations (21) and (38). The other alternative is to consider a special case for which the equations can be solved analytically and this is what we will do here.

We consider the case $\Delta t = t$, $n = 1$, and $T = 0$. From (37a) we see that then E_k does not depend on k and from the equation (21) relating n and $\widetilde{\mu}$ it follows that $E_k = 0$. Assuming a non-trivial solution $\Delta_k \neq 0$, $f_k = (a + b \cos k)^{-1}$ we find, after some straightfoward algebra,

$$a = -\frac{U}{2} \quad ; \quad b = -2\Delta t \quad ; \quad \text{for} \quad |U| > 4|t| \quad . \tag{41}$$

The corresponding ground-state energy is $UL/2$, which is the exact ground-state energy for $U < -4t$ and $n = 1$.[44–46] The on-site pairing correlation function is given by

$$P_0 = (L+1)/4 \quad ; \quad |U| > 4|t| \quad , \tag{42}$$

so that there is also ODLRO in this case. Although at first sight, there may be a flow of particles because $t \neq 0$, closer inspection reveals that the current operator acting on the ground state (with ODLRO) is identically zero, hence also this state is not superconducting. This is due to our choise $\Delta t = t$ which implies the strict conservation of local pairs of particles. As for the Hubbard model in the atomic limit, the BCS treatment of model (34) yields the exact ground-state energy[44–46] for $\Delta t = t$, $n = 1$ and $U < -4t$. Note that for $U > 4|t|$ the ground-state energy is also given by $UL/2$ and that there is also ODLRO in this case. However, the ground-state energy given by the BCS treatment of model (34) is larger than the exact ground-state energy which is zero in this parameter regime.[44–46]

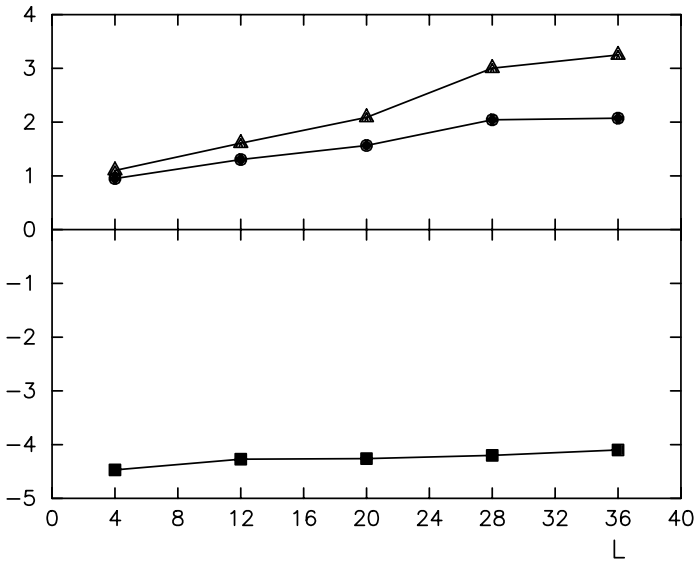

Fig.8. Ground-state energy per site E/L, on-site pairing correlation function P_0 and largest eigenvalue λ_0 of the reduced two-particle density matrix as a function of system size L for the Hubbard model with correlated hopping for $t = 1$, $\Delta t = 0.4$, $U = 0$ and $n = 1.5$. Squares: $10E/L$; bullets: P_0; triangles: λ_0. The lines are guides to the eye.

5.2 Numerical results

Our SD results for the Hubbard model with correlated hopping for $\Delta t = t$ and $n = 1$ for rings of various lengths (results not shown) indicate that for $U > U_c$ the ground-state energy is zero and that no on-site electron pairs are formed. For $U < -U_c$ all electrons are paired, the pairs are static and the ground-state energy is equal to the number of pairs times U. For $L = 6$, $U_c = 3.5$; for $L = 10$, $U_c = 3.9$ and for rings with fourteen or more sites $U_c = 4$. All these results are in perfect agreement with the analytical results obtained in the thermodynamic limit.[43−46]

We have already seen that ODLRO may show up if the system prefers to form pairs and if the ground-state is highly degenerate, as in the $\Delta t = t$ case. It is of interest to explore the possibility of ODLRO in less "symmetrical" or non-perturbative cases. For $n > 1$ the correlated hopping interaction may be attractive and may favor the formation of (extended) pairs, as can be seen from a simple Hartree-Fock argument. For $U = 0$ the weak-coupling ($0 < U \ll t$, $0 < \Delta t \ll t$) continuum-limit theory[48] yields singlet superconducting correlations if

$$\frac{4\Delta t}{\pi t} \operatorname{cotg} \frac{n\pi}{2} < 0 \quad . \tag{43}$$

Guided by (43) we take $\Delta t = 0.4$, $t = 1$ and $n = 3/2$.

Numerical results for the ground-state energy per site E/L, the on -site pairing

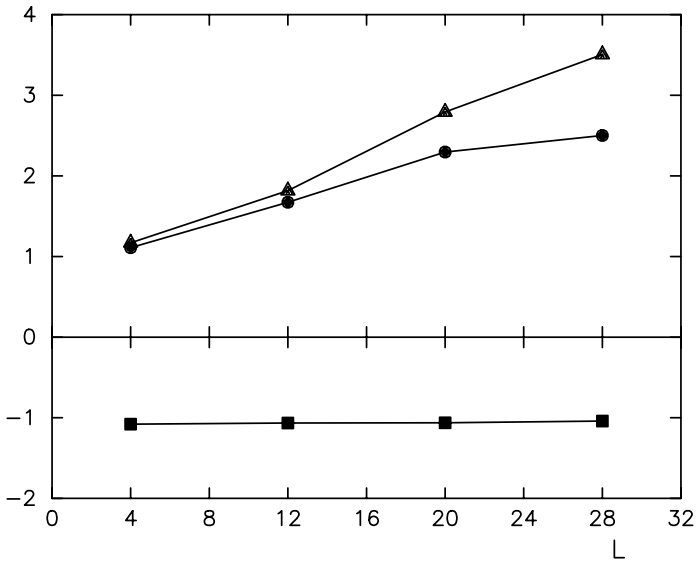

Fig.9. Ground-state energy per site E/L, on-site pairing correlation function P_0 and largest eigenvalue λ_0 of the reduced two-particle density matrix as a function of system size L for the Hubbard model with correlated hopping for $t = 1$, $\Delta t = 0.4$, $U = -1$ and $n = 1.5$. Squares: E/L; bullets: P_0; triangles: λ_0. The lines are guides to the eye.

correlation function P_0 and the largest eigenvalue λ_0 of the two-particle density matrix as a function of system size for the three quarter filled Hubbard model with correlated hopping are shown in Figs. 8-11. The number of important states M_I collected by the SD algorithm, working in the Fourier space representation, varies from $M_I = 4$ for $L = 4$ to $M_I \approx 192000$ for $L = 36$. In the latter case the dimension of the Hilbert space $M \approx 8.2\,10^{19}$, so that $M_I \ll M$ indeed.

For $U = 0$ and $12 \leq L < 36$ the ground-state energy changes little with L, as seen from Fig.8. The largest eigenvalue λ_0 of the two-particle density matrix increases with L, indicating that the system exhibits ODLRO, in concert with theory.[48] The on-site pairing correlation function P_0 also increases with L but is much smaller than λ_0. From the eigenvector of the two-body density matrix, corresponding to λ_0, it follows that the ODLRO is mainly of the extended s-wave type.

For $U = -1$ and $4 \leq L < 28$ the ground-state energy is almost constant, as seen from Fig.9. The largest eigenvalue λ_0 of the two-particle density matrix increases with L, indicating that the system exhibits ODLRO. Also in this case the on-site pairing correlation function P_0 increases with L but is much smaller than λ_0. Hence, the ODLRO is not of the pure on-site (s-wave) type. From the eigenvector of the two-body density matrix, corresponding to λ_0, it follows that the ODLRO is mainly of the extended s-wave type.

As seen from Figs. 10 and 11, for $U = 0.5$ and $U = 1$ the behavior of E/L, P_0 and λ_0 as a function of L is qualitatively the same as for $U = 0$ and $U = -1$, respectively.

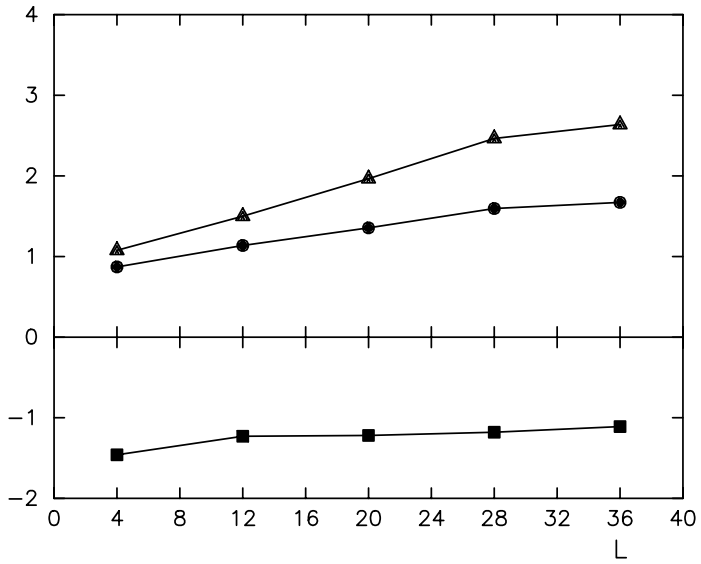

Fig.10. Ground-state energy per site E/L, on-site pairing correlation function P_0 and largest eigenvalue λ_0 of the reduced two-particle density matrix as a function of system size L for the Hubbard model with correlated hopping for $t = 1$, $\Delta t = 0.4$, $U = 0.5$ and $n = 1.5$. Squares: $10E/L$; bullets: P_0; triangles: λ_0. The lines are guides to the eye.

Also in these cases we find strong evidence for ODLRO of the extended s-wave type, and this in a parameter regime where there is no special symmetry in the model and for which the continuum theory[48] does not apply. To the best of our knowledge this is the first demonstration, not based on a BCS treatment, that correlated hopping terms can lead to ODLRO in a system of electrons with a repulsive on-site interaction. Since for small U we find ODLRO in the Hubbard model with correlated hopping whereas for the standard model we do not find ODLRO, it seems that the correlated hopping interaction not only favors the formation of pairs but also reduces the size of the electron pairs.

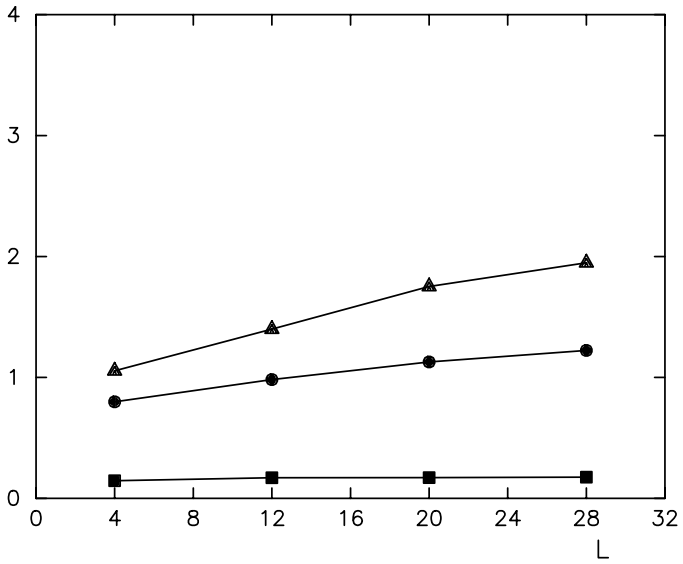

Fig.11. Ground-state energy per site E/L, on-site pairing correlation function P_0 and largest eigenvalue λ_0 of the reduced two-particle density matrix as a function of system size L for the Hubbard model with correlated hopping for $t = 1$, $\Delta t = 0.4$, $U = 1$ and $n = 1.5$. Squares: E/L; bullets: P_0; triangles: λ_0. The lines are guides to the eye.

6. Conclusions

The stochastic diagonalization technique has been employed to examine the conditions under which models for interacting electrons on a lattice exhibit Off-Diagonal Long-Range Order. Analytical results for some limiting cases show that a system can support Off-Diagonal Long-Range Order without being a superconductor. On the basis of our results we conjecture that the (repulsive) Hubbard model, supplemented with correlated hopping terms, exhibits Off-Diagonal Long-Range Order for a wide range of model parameters.

7. Acknowledgements

We would like to thank W. Fettes for critical comments on the manuscript. Financial support by the Human Capital and Mobility program of the EEC, the "Stichting voor Fundamenteel Onderzoek der Materie (FOM)", which is financially supported by the "Nederlandse Organisatie voor Wetenschappelijk Onderzoek (NWO)", and the "Stichting Nationale Computer Faciliteiten (NCF)" is gratefully acknowledged.

8. References

1. O. Penrose, *Phil. Mag.* **42** (1951) 1373.
2. O. Penrose, and L. Onsager, *Phys. Rev.* **104** (1956) 576.
3. C.N. Yang, *Rev. Mod. Phys.* **34** (1962) 694.
4. G.L. Sewell, *J. Stat. Phys.* **61** (1990) 415.
5. H.T. Nieh, Gang Su, Bao-Heng Zhao, *Phys. Rev.* **B51** (1995) 3760.
6. Chi Au, Bao-Heng Zhao, *Phys. Lett.* **A209** (1995) 235.
7. P.C. Hohenberg, *Phys. Rev.* **158** (1967) 383.
8. C.N. Yang, *Phys. Rev. Lett.* **63** (1989) 2144.
9. H. Betsuyaku, *Phys. Rev.* **B44** (1991) 871.
10. R.R.P. Singh, and R.T. Scalettar, *Phys. Rev. Lett.* **66** (1991) 3203.
11. E. Dagotto, *Rev. Mod. Phys.* **66** (1994) 763.
12. E. Dagotto, and A. Moreo, *Phys. Rev.* **D21** (1985) 865.
13. E. Gagliano, E. Dagotto, A. Moreo, and F. Alcaraz, *Phys. Rev.* **B34** (1986) 1677; *Phys. Rev.* **B35** (1986) 5297.
14. G. Fano, F. Ortolani, and F. Semeria, *Int. J. Mod. Phys.* **B3** (1990) 1845.
15. G. Fano, F. Ortolani, and A. Parola, *Phys. Rev.* **B46** (1992) 1048.
16. E. Dagotto, A. Moreo, F. Ortolani, D. Poilblanc, and J. Riera, *Phys. Rev.* **B45** (1992) 10741.
17. K.E. Schmidt, and D.M. Ceperley, *Monte Carlo Methods in Condensed Matter Physics*, edited by K. Binder, (Springer, Berlin, 1992).
18. H. De Raedt and W. von der Linden, *Monte Carlo Methods in Condensed Matter Physics*, edited by K. Binder, (Springer, Berlin, 1992).
19. H. De Raedt, and W. von der Linden, *Phys. Rev.* **B45** (1992) 8787.
20. H. De Raedt, and M. Frick, *Phys. Rep.* **231** (1993) 107.
21. J.H. Wilkinson, *The Algebraic Eigenvalue Problem*, (Clarendon Press, Oxford, 1965).
22. B.N. Parlett, *The Symmetric Eigenvalue Problem*, (Prentice-Hall, New Jersey, 1981).
23. W. von der Linden, *Phys. Rep.* **220** (1992) 53.
24. N. Byers and C.N. Yang, *Phys. Rev. Lett.* **7** (1961) 46.
25. D.J. Scalapino, S.R. White, and S. Zhang, *Phys. Rev.* **B47** (1993) 7995.
26. F. London, *J. Phys. Rad.* **8** (1937) 397.
27. M. Büttiker, Y. Imry, and R. Landauer, *Phys. Lett.* **96A** (1983) 365.
28. H.F. Cheung, E. Riedel, and Y. Gefen, *Phys. Rev. Lett.* **62** (1989) 587.
29. H. Bouchiat and G. Montambaux, *J. Phys. (Paris)* **50** (1989) 2695.
30. L.P. Lévy, G. Dolan, J.Dunsmir, and H. Bouchiat, *Phys. Rev. Lett.* **64** (1990) 2074.
31. M.E. Fisher, M.N. Barber, and D. Jasnow, *Phys. Rev.* **A8** (1973) 1111.
32. P.J.H. Denteneer, Guozhong An, and J.M.J. van Leeuwen, *Phys. Rev.* **B47**

(1993) 6256.
33. F.F. Assaad, W. Hanke, and D.J. Scalapino, *Phys. Rev.* **B50** (1994) 12835.
34. J.M.J. van Leeuwen, M.S.L. du Croo de Jongh, and P.J.H. Denteneer, *J. Phys. A: Math. Gen.* **29** (1996) 41.
35. Similar conclusions follow for a two- or three-dimensional system.
36. C.A. Stafford, A.J. Millis, and B.S. Shastry, *Phys. Rev.* **B43** (1991) 13660.
37. R.M. Feye, M.J. Martins, D.J. Scalapino, J. Wagner, and W. Hanke, *Phys. Rev.* **B44** (1991) 6909.
38. Although we presented some results for a one-dimensional system only, the same conclusion holds for a two- or three-dimensional system.
39. R.J. Bursill and C.J. Thompson, *J. Phys. A: Math. Gen.* **26** (1993) 769.
40. G.D. Mahan, *Many-Particle Physics*, (Plenum Press, New York, 1981).
41. J. Hubbard, *Proc. Roy. Soc. London A* **276** (1963) 238.
42. L.G. Caron and G.W. Pratt Jr., *Rev. Mod. Phys.* **40** (1968) 802.
43. R. Strack, and D. Vollhardt, *Phys. Rev. Lett.* **70** (1993) 2637.
44. A.A. Ovchinnikov, *J. Phys.: Condens. Matter* **6** (1994) 11057.
45. L. Arrachea, and A.A. Aligia, *Phys. Rev. Lett.* **73** (1994) 2240.
46. A. Schadschneider, *Phys. Rev.* **B51** (1995) 10386.
47. L. Arrachea, A.A. Aligia, E. Gagliano, K. Hallberg, and C. Balseiro, *Phys. Rev.* **B50** (1994) 16044.
48. G. Japaridze, and E. Müller-Hartmann, *Ann. Physik* **3** (1994) 163.
49. J.E. Hirsch, *Physica* **C158** (1989) 326.
50. J.E. Hirsch, *Phys. Lett.* **A138** (1989) 83.
51. H.B. Schüttler, and A.J. Fedro, *Phys. Rev.* **B45** (1992) 7588.
52. M.E. Simón, M. Baliña, and A.A. Aligia, *Physica* **C206** (1993) 297.
53. M.E. Simón, and A.A. Aligia, *Phys. Rev.* **B48** (1993) 7471.
54. R.E. Lagos, G.A. Lara, and G.G. Cabrera, *Phys. Rev.* **B47** (1993) 12445.
55. R. Micnas, J. Ranninger, and S. Robaszkiewicz, *Phys. Rev.* **B39** (1989) 11653.
56. G.A. Lara, and G.G. Cabrera, *Phys. Rev.* **B47** (1993) 14417.
57. F.D. Buzatu, *Int. J. Mod. Phys.* **B9** (1995) 1503.
58. J.E. Hirsch, and F. Marsiglio, *Phys. Rev.* **B34** (1989) 11515.
59. F. Marsiglio, and J.E. Hirsch, *Physica* **C171** (1990) 554.
60. J.E. Hirsch and F. Marsiglio, *Phys. Rev.* **B41** (1990) 2049.
61. J. de Boer, V.E. Korepin, and A. Schadschneider, *Phys. Rev. Lett.* **74** (1995) 789.
62. L. Arrachea, A.A. Aligia and E. Gagliano, *Phys. Rev. Lett.* **76** (1996) 4396.
63. K. Michielsen, H. De Raedt, and T. Schneider, *Phys. Rev. Lett.* **68** (1992) 1410.
64. K. Michielsen, *Int. J. Mod. Phys.* **B7** (1993) 2571.
65. P. de Vries, K. Michielsen, and H. De Raedt, *Phys. Rev. Lett.* **70** (1993)

2463.
66. P. de Vries, K. Michielsen, and H. De Raedt, *Z. Phys.* **B92** (1993) 353.
67. K. Michielsen, H. De Raedt, T. Schneider, and P. de Vries, *Europhys. Lett.* **25** (1994) 599.
68. P. de Vries, K. Michielsen and H. De Raedt, *Z. Phys.* **B95** (1994) 475.
69. K. Michielsen, *Phys. Rev.* **B50** (1994) 4283.
70. K. Michielsen, and H. De Raedt, *Phys. Rev.* **E50** (1994) 4371.